


Generation of isolated attosecond pulses in a multi-cycle inhomogeneous two-color field without CEP stabilization

Hua Yuan¹ · Lixin He¹  · Feng Wang¹ · Baoning Wang¹ · Weiwei Liu¹ · Zuofei Hong²

Received: 18 January 2017 / Accepted: 10 May 2017
© Springer Science+Business Media New York 2017

Abstract We theoretically demonstrate the generation of ultrashort isolated attosecond pulses (IAPs) in the water window region with a multi-cycle inhomogeneous two-color field synthesized by an 800-nm fundamental pulse and a 2000-nm control pulse. The results show that the high-order harmonic generation process is effectively controlled in the temporally and spatially shaped field. An ultra-broadband supercontinuum in the water window region with the photon energies ranging from 387 to 620 eV is generated. Such a supercontinuum supports the generation of an ultrashort IAP with a duration as short as 40 attosecond. Moreover, we analyze the influence of the carrier-envelope phases (CEPs) and the relative phase of the two-color field on the IAP generation. It is shown that our two-color scheme is robust for the generation of sub-80 as IAPs against variations of the CEPs and the relative phase.

Keywords Isolated attosecond pulse · High-order harmonic generation · Multi-cycle inhomogeneous two-color field · Water window

1 Introduction

High-order harmonics are generated when atoms or molecules are irradiated with an intense laser field. HHG has been used for the production of coherent extreme ultraviolet (EUV) and soft X-ray sources (Chang et al. 1997; Popmintchev et al. 2012; Teichmann et al. 2016), as well as the generation of attosecond pulses (Corkum and Krausz 2007;

✉ Lixin He
helx@mail.hust.edu.cn

¹ School of Physics and Wuhan National Laboratory for Optoelectronics, Huazhong University of Science and Technology, Wuhan 430074, China

² Laboratory of Optical Information Technology, Wuhan Institute of Technology, Wuhan 430205, China

Krausz and Ivanov 2009; Lan et al. 2007; Paul et al. 2001; Zhang et al. 2017; Li et al. 2017a). These ultrashort pulses have served as an important tool for probing and controlling electronic dynamics in atoms, molecules and solids (Itatani et al. 2004; Zhai et al. 2016; Qin and Zhu 2017; Zhai et al. 2017; Goulielmakis et al. 2010; Zhu et al. 2016; Ma et al. 2017; He et al. 2016; Zhou et al. 2017; Li et al. 2017b; Liu et al. 2017a; Cavalieri et al. 2007) with unprecedented temporal resolution. Owing to these potential applications, HHG and attosecond pulse generation have been a topic of great interest in the past years.

The physical mechanism of HHG can be well explained by the three-step model (Corkum 1993): ionization, acceleration, and recombination. During the recombination, the highest photon energy obeys the cutoff law, $I_p + 3.17U_p$, where I_p is the ionization potential, and $U_p \propto I\lambda^2$ is the ponderomotive energy. This process is restricted to a single half an optical cycle, which results in the generation of an attosecond pulse train with a periodicity of half an optical cycle (Paul et al. 2001). Since straightforward attosecond metrology usually prefers an IAP to an attosecond pulse train, it has stimulated much effort to produce an IAP. One of the pioneer works is using a few-cycle driving pulse (Hentschel et al. 2001; Kienberger et al. 2004; Goulielmakis et al. 2008). With this method, the emission time of the highest harmonic can be confined within half an optical cycle where the laser field reaches its maximum. This can lead to a supercontinuum at the cutoff and then an IAP can be filtered out. However, the requirement of the few-cycle driving pulse for the generation of IAPs is rather stringent: a few-cycle pulse with a stabilized CEP is required. Therefore, some other methods, such as the polarization gating technique (Chang 2005; Sansone et al. 2006), two-color and multicolor driving fields (Pfeifer et al. 2006; Lan et al. 2009; Takahashi et al. 2010, 2013; Lan et al. 2010; Haessler et al. 2014, 2015; Li et al. 2017c), have been proposed. In particular, by using a mid-infrared (MIR) pulse in combination of the above methods, the harmonic spectrum can be effectively extended, even to the water window region [a spectral range between the K-absorption edges of carbon (284 eV) and oxygen (543 eV)] (Takahashi et al. 2008), which has an important application for imaging living specimens in biology.

Recently, the plasmonic field-enhanced HHG has attracted much attention. When a low-intensity laser pulse from the femtosecond oscillator is directly focused onto a narrow metallic nanostructure, the intensity of the incident field is boosted in the vicinity of the nanostructure due to the surface plasmon resonances (Kim et al. 2008; Sivis et al. 2012; Zhao et al. 2017; Liu et al. 2017b; Ke et al. 2017). The enhanced laser intensity easily exceeds the threshold intensity for HHG in noble gases without extra cavities to amplify the input laser power (Kim et al. 2008; Sivis et al. 2012; Kim et al. 2012; Park et al. 2011; Sivis et al. 2013). Due to the strong confinement of the plasmonic hot spots, the enhanced laser field is not spatially homogeneous in the region where the electron dynamics take place. Consequently, it leads to important changes in the HHG process. By exploiting the enhanced field based on surface plasmon resonances, Kim et al. (2008) first observed HHG with bow-tie-shaped nanostructures. The harmonics with wavelengths from 47 nm (17th) to 114 nm (7th) have been successfully produced. But it should be stressed here that the outcomes of this experiment are controversial (Sivis et al. 2012; Kim et al. 2012). Using nearly identical experimental conditions, Sivis et al. (2012) only observed line emission of neutral and ionized gas atoms, instead of HHG. Fortunately, alternative approaches to realize plasmonic field enhancement for HHG were explored by employing different kinds of nanostructures (Park et al. 2011). Due to the spatial variation at a nanometer scale of the enhanced laser field, HHG driven by the inhomogeneous field shows some different characteristics (Luo et al. 2013; Yavuz et al. 2012; Ciappina et al. 2012; Pérez-Hernández

et al. 2013; Shaaran et al. 2013; He et al. 2013), for example, the generation of even order harmonics, the extension of the cutoff and the selection of a single quantum path. Recently, it has been proposed to generate IAPs with the inhomogeneous field (Luo et al. 2013; Yavuz et al. 2012).

In this paper, we propose to generate an ultrashort IAP in the water window region with a multi-cycle inhomogeneous two-color field, which is synthesized by a near-infrared (NIR) 800-nm fundamental pulse and a weaker 2000-nm (MIR) control field. Based on the numerical solution of the time-dependent Schrödinger equation (TDSE) in one spatial dimension (1D), we demonstrate that the harmonic spectrum generated in this two-color field is extended to 620 eV, and a 233-eV supercontinuum (387–620 eV) spanning the water window is straightforwardly produced. By superposing harmonics in the broadband supercontinuum, a 40-as IAP is obtained in the water window region. Moreover, we have also discussed the influences of the CEPs and the relative phase of the two incident laser pulses on the generation of the IAP. The results show that broadband supercontinua ranging from 543 to 620 eV can be produced for almost all the values of CEPs and relative phases. Then IAPs with durations below 80 as can be created without the requirement of the stabilization of both the CEPs and the relative phase.

2 Theoretical model

In our simulations, the harmonic spectrum is calculated by solving the 1D-TDSE, which reads (atomic units are used throughout)

$$\begin{aligned}
 i \frac{\partial \psi(x, t)}{\partial t} &= H(x, t) \psi(x, t) \\
 &= \left[-\frac{1}{2} \frac{\partial^2}{\partial x^2} + V_{atom}(x) + V_{laser}(x, t) \right] \psi(x, t).
 \end{aligned}
 \tag{1}$$

Here $V_{atom}(x) = -\frac{1}{\sqrt{x^2 + \alpha}}$ is the soft-core potential. The soft core parameter α is chosen to be 0.667 to match the ground ionization potential of the neon atom, which is 0.7925 a.u. $V_{laser}(x, t) = -E(x, t)x$ is the potential due to the laser-electron interaction. The inhomogeneous field is given by Yavuz et al. (2012), Pérez-Hernández et al. (2013)

$$E(x, t) = E_t(t)(1 + \varepsilon x).
 \tag{2}$$

The parameter ε determines the strength of the spatial inhomogeneity of the laser field. For example, $\varepsilon = 0.003$ means the field intensity varies by 0.3% over 1 a.u. length. Such a spatial inhomogeneity parameter can be easily accomplished by using the gold bow-tie-shaped nanostructure (Ciappina et al. 2012; Pérez-Hernández et al. 2013).

In our simulations, the multi-cycle two-color field is synthesized by a 30-fs, 800-nm (NIR) fundamental pulse and a 30-fs, 2000-nm (MIR) control pulse, which can be written as

$$\begin{aligned}
 E_t(t) &= E_0 f(t) \cos \left[\omega_0 \left(t - \frac{T}{2} \right) + \phi_0 \right] \\
 &+ E_1 f(t) \cos \left[\omega_1 \left(t - \frac{T}{2} \right) + \phi_1 - \Delta\phi \right].
 \end{aligned}
 \tag{3}$$

Here E_0 , E_1 and ω_0 , ω_1 are the amplitudes and the frequencies of the fundamental pulse and the control pulse, respectively. ϕ_0 and ϕ_1 are the CEPs of the fundamental pulse and the control pulse, respectively. $\Delta\phi$ is the relative phase between the fundamental pulse and the control pulse. In experiments, the MIR control pulse can be generated from the white-light continuum (WLC) seeded optical parametric amplifier (OPA) system. The CEPs of the fundamental and control pulses obey the phase property of the WLC-seeded OPA, i.e., $\phi_1 = \phi_0 + \frac{\pi}{2}$ (Baltuška et al. 2002). $f(t) = \sin^2(\frac{\pi t}{T})$ is the pulse envelope. $T = 30T_0$, T_0 is the optical cycle of the 800-nm pulse.

We use the split-operator method to solve Eq. (1) (Feit et al. 1982). The neon atom is in the initial state (ground state) before we turn on the laser. The ground state is obtained by imaginary time propagation with the soft-core potential. Then time-dependent dipole acceleration can be obtained by

$$a(t) = \frac{d^2\langle x \rangle}{dt^2} = -\langle \psi(x, t) | [H(x, t), [H(x, t), x]] | \psi(x, t) \rangle. \quad (4)$$

By Fourier transforming the time-dependent dipole acceleration, we can get the harmonic spectrum, which is given by

$$I_q = |a_q(\omega)|^2 = \left| \frac{1}{T} \int_0^T a(t) e^{-iq\omega t} dt \right|^2. \quad (5)$$

The attosecond pulse can be obtained by superposing several orders of harmonics,

$$I(t) = \left| \sum_q a_q e^{iq\omega t} \right|^2. \quad (6)$$

Here q corresponds to the harmonic order.

It is worth mentioning that a more accurate method to calculate the harmonic spectrum should be solving the three-dimensional (3D) TDSE. However, in our simulations, the incident laser is linearly polarized, the dynamics of the atomic electron are mainly along the polarization direction of the laser field. It is reasonable to model the HHG process by solving the 1D-TDSE. We have also calculated the harmonic spectrum by the 3D model. We find that the harmonic spectrum obtained by the 1D model is in good agreement with that obtained by the 3D model, but the harmonics intensities obtained by the 1D model are slightly higher than that obtained by the 3D model. This is because the lateral spreading of the electron wave packet is ignored in the 1D model. However, such a slight difference will not change our conclusion.

3 Results and discussion

We first investigate the HHG process in a 30-fs, 800-nm (NIR) fundamental field. The intensity I_0 and CEP ϕ_0 of the laser pulse are 3.0×10^{14} W/cm² and 0, respectively. The inhomogeneity parameter ε is chosen to be 0.003. The electric field is shown in Fig. 1a. Figure 1b, c are the calculated harmonic spectrum and the corresponding time-frequency distribution. As can be seen in Fig. 1c, within per half an optical cycle, there are two dominant branches with comparable intensity contributing to the harmonic emission, which are called the short and long quantum paths. Owing to the interference of these

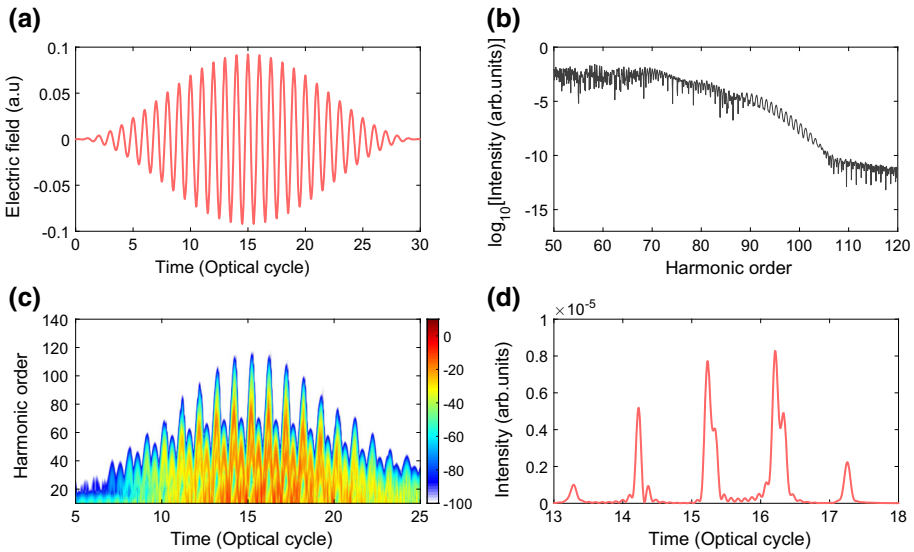


Fig. 1 (Color online) **a** The electric field of the 30-fs, 800-nm one-color field. **b** and **c** are the harmonic spectrum and the corresponding time-frequency distribution in the multi-cycle one-color inhomogeneous field with $\varepsilon = 0.003$. **d** The temporal profiles of attosecond pulses generated by synthesizing the harmonics from 124 eV (80th) to 140 eV (90th)

quantum paths, the harmonic spectrum exhibits modulation structures in the plateau [see Fig. 1b]. Moreover, one can also see that the energy difference between the highest and second-highest radiation peaks, which determines the bandwidth of the harmonic continuum, is virtually invisible. Therefore, one can barely obtain a supercontinuum in the spectrum presented in Fig. 1b. By superposing the harmonics from 124 eV (80th) to 140 eV (90th) in the cutoff region, we can only obtain an attosecond pulse train rather than an IAP, as shown in Fig. 1d.

To generate an IAP in the multi-cycle regime, we consider modulating the electron dynamics by adding a 30-fs, 2000-nm (MIR) control pulse to the fundamental pulse. In our scheme, the intensity of the control pulse is 20% of the fundamental pulse, i.e., $6 \times 10^{13} \text{ W/cm}^2$. The CEPs ϕ_0 , ϕ_1 , and the relative phase $\Delta\phi$ are set to be 0, 0.5π and 0.5π , respectively. The inhomogeneity parameter ε is taken as 0.003. Figure 2a shows the electric fields of the fundamental field (black dashed line), the control field (green solid line), and the synthesized two-color field (red solid line). Figure 2b presents the harmonic spectrum generated in the synthesized two-color field. One can clearly see that, due to the addition of the 2000-nm control pulse, the cutoff of the harmonic spectrum is extended to 620 eV (400th harmonic) and a smooth supercontinuum with a bandwidth of 233 eV [from 387 eV (250th) to 620 eV (400th)] in the water window region is successfully produced. For a deeper insight, we have performed the time-frequency analysis of the harmonic spectrum. As shown in Fig. 2c, the harmonics above 233 eV (150th) are dominated by three main emission peaks (marked as R_1 , R_2 , and R_3) around $t = 10T_0$, $15T_0$, $20T_0$, respectively. Among them, the maximum energy of the highest emission peak R_2 reaches 620 eV (400th), corresponding to the harmonic cutoff in Fig. 2b. While for the emission peaks R_1 and R_3 , the maximum energies are only 387 eV (250th). Therefore, harmonics from 387 eV (250th) to 620 eV (400th) become continuous, forming the broadband

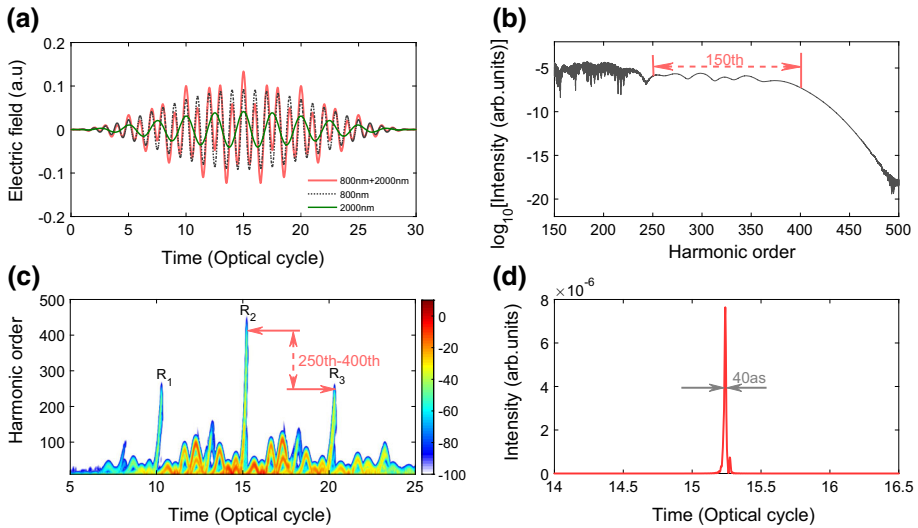


Fig. 2 (Color online) **a** The electric fields of the 30-fs, 800-nm fundamental pulse (*black dashed line*), 30-fs, 2000-nm control pulse (*green solid line*) and the synthesized two-color field (*red solid line*). **b** and **c** are the harmonic spectrum and the corresponding time-frequency distribution in the multi-cycle two-color inhomogeneous field with $\varepsilon = 0.003$. **d** The temporal profile of the IAP generated by synthesizing the harmonics from 480 eV (310th) to 605 eV (390th) in the supercontinuum

233-eV supercontinuum in the water window region. Besides, we find that for all the three emission peaks, only short quantum paths survive. This is because the spatial inhomogeneity of the laser field can force the long quantum path to converge with the short one. The flight time of the long quantum path is larger than that of the short one, the efficiency of the long one is much lower (Yavuz et al. 2012; Ciappina et al. 2012), thus the modulation in the supercontinuum is significantly reduced. Such a smoothly broadband supercontinuum can be used to generate an IAP in the water window region. Figure 2d shows the IAP obtained by superposing the harmonics from 480 eV (310th) to 605 eV (390th), of which the pulse duration is as short as 40 attosecond.

Next, we investigate the role of the inhomogeneity of the field with three different inhomogeneity parameters. In our simulations, except for the inhomogeneity parameter, other parameters are the same as that in Fig. 2. Figure 3a, b show the harmonic spectrum and the corresponding time-frequency analysis with the inhomogeneity parameter $\varepsilon = 0$, i.e., the case of homogeneous field. As can be seen from Fig. 3b, the maximum energy of the highest radiation peak R_2 is 23 eV higher than that of the second-highest radiation peak R_1 . Thus a 23-eV (140th–155th) supercontinuum is generated as shown in Fig. 3a. Moreover, due to the coexistence of short and long quantum paths, the supercontinuum region exhibits modulations. Such a supercontinuum is difficult to produce an IAP with a duration less than 100 as. While in the case of $\varepsilon = 0.0015$ [Figs. 3c, d], the harmonic cutoff is obviously extended to 372 eV (240th) when compared with that [240 eV (155th)] in Fig. 3b. This is because that in the spatially inhomogeneous field, the electric field $E(x, t) = E_t(t)(1 + \varepsilon x)$ varies with the distance x between the released electron and its parent ion ($x = 0$ refers to the position for the parent ion). Thus the free electrons gain more kinetic energies in the acceleration process and then give rise to the harmonic cutoff extension (Yavuz et al. 2012). Moreover, in Fig. 3d, we can see that the maximum kinetic

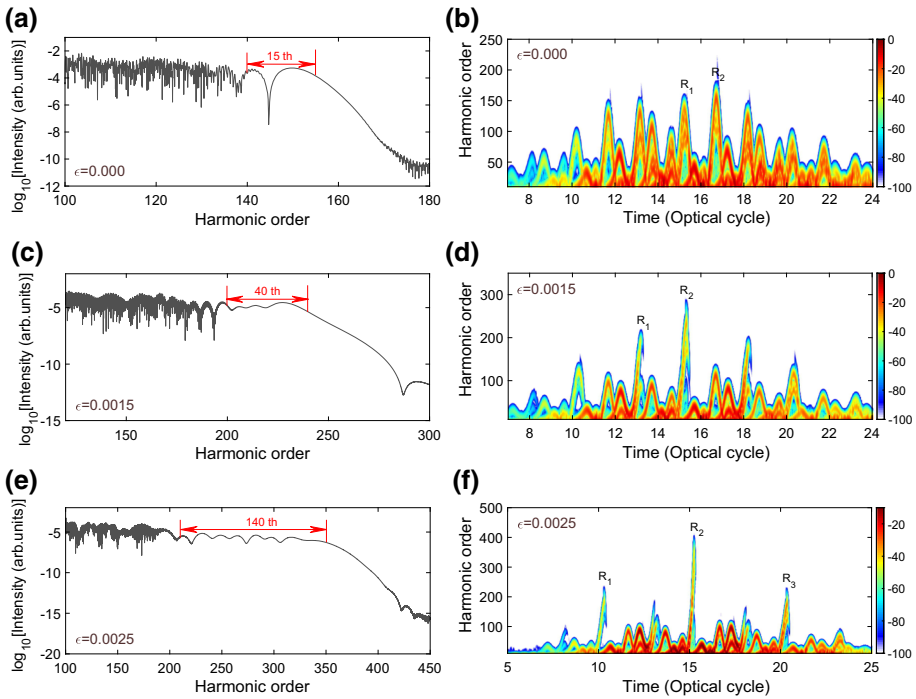


Fig. 3 (Color online) The harmonic spectra in the multi-cycle two-color field with different inhomogeneity parameters: **a** $\varepsilon = 0.000$, **c** $\varepsilon = 0.0015$ and **e** $\varepsilon = 0.0025$. **b**, **d** and **f** are the corresponding time-frequency analyses to **(a)**, **(c)** and **(e)**, respectively. In our simulations, except for the inhomogeneity parameter, other parameters are the same as that in Fig. 2

energy of the highest radiation peak R_2 is 372 eV (240th), while that of the second-highest radiation peak R_1 is 310 eV (200th).

Therefore, a supercontinuum with the bandwidth of 62 eV (200th–240th) is generated as shown in Fig. 3c. As the ε increased to 0.0025, the maximum kinetic energy of the highest radiation peak R_2 is further extended to 543 eV (350th), which is 217 eV higher than that [326 eV (210th)] of the second-highest peak R_1 or R_3 (Fig. 3f). Therefore, a broadband supercontinuum in the region from 326 eV (210th) to 543 eV (350th) is generated as shown in Fig. 3e.

In the following, we investigate the CEPs dependence of the IAP generation in the multi-cycle inhomogeneous two-color field. In our simulations, the CEP ϕ_0 of the 800-nm pulse changes from 0 to 2π , in the meantime, the CEP of the 2000-nm pulse ϕ_1 is $\phi_0 + 0.5\pi$. Except for ϕ_0 and ϕ_1 , other parameters are the same as that in Fig. 2. In Fig. 4a, we show the CEPs-dependent harmonic spectra in the multi-cycle inhomogeneous two-color field. It is worth mentioning that in a homogeneous field, because of the inversion symmetry, the harmonic spectra of $\phi_0 = 0$ and $\phi_0 = \pi$ are exactly the same.

However, in inhomogeneous field, the inversion symmetry is broken and the harmonic spectra of $\phi_0 = 0$ and $\phi_0 = \pi$ are different (Yavuz et al. 2012). The spectral profiles and cutoff positions are different when ϕ_0 changes from 0 to 2π (see in Fig. 4a). Even so, we find that supercontinua with the spectral ranges from 543 eV (350th) to 620 eV (400th) can still be generated for all the values of ϕ_0 . We further investigate the CEPs effect on the IAP

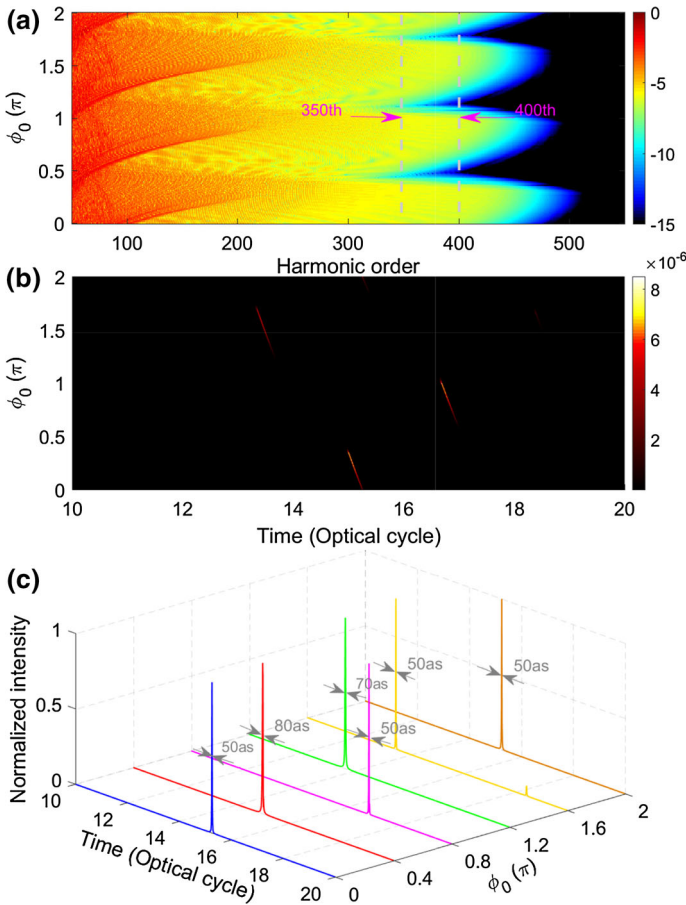


Fig. 4 (Color online) **a** The CEPs dependence of the generated harmonic spectrum in the multi-cycle two-color inhomogeneous field. The *color bar* shows the harmonic spectrum in a logarithmic scale. **b** The CEPs dependence of the IAP generated by synthesizing the harmonics from 543 eV (350th) to 620 eV (400th). **c** Temporal profiles of the IAPs with different CEPs (0π , 0.4π , 0.8π , 1.2π , 1.6π , 2.0π). In our simulations, except for ϕ_0 and ϕ_1 , other parameters are the same as that in Fig. 2

generation by superposing the harmonics from 543 eV (350th) to 620 eV (400th). As shown in Fig. 4b, the IAPs can be obtained for all the values of ϕ_0 . In Fig. 4c, we show that the temporal profiles of IAPs in the cases of $\phi_0 = 0, 0.4\pi, 0.8\pi, 1.2\pi, 1.6\pi, 2.0\pi$. It is shown that the IAPs below 80 as can be obtained.

Finally, we investigate the effect of the relative phase on the generation of the IAP. In our simulations, the relative phase $\Delta\phi$ changes from 0 to 2π , other parameters are the same as that in Fig. 2. Figure 5a shows the relative phase dependence of harmonic spectrum. One can clearly see that the harmonic spectra show a sensitive dependence on $\Delta\phi$. The cutoff position changes as $\Delta\phi$ varies from 0 to 2π . But the supercontinua ranging from 543 eV (350th) to 620 eV (400th) can still be obtained in a broad range of relative phases. The relative phase dependence of the IAP generated by superposing the broadband supercontinuum from 543 eV (350th) to 620 eV (400th) is presented in Fig. 5b. One can see that,

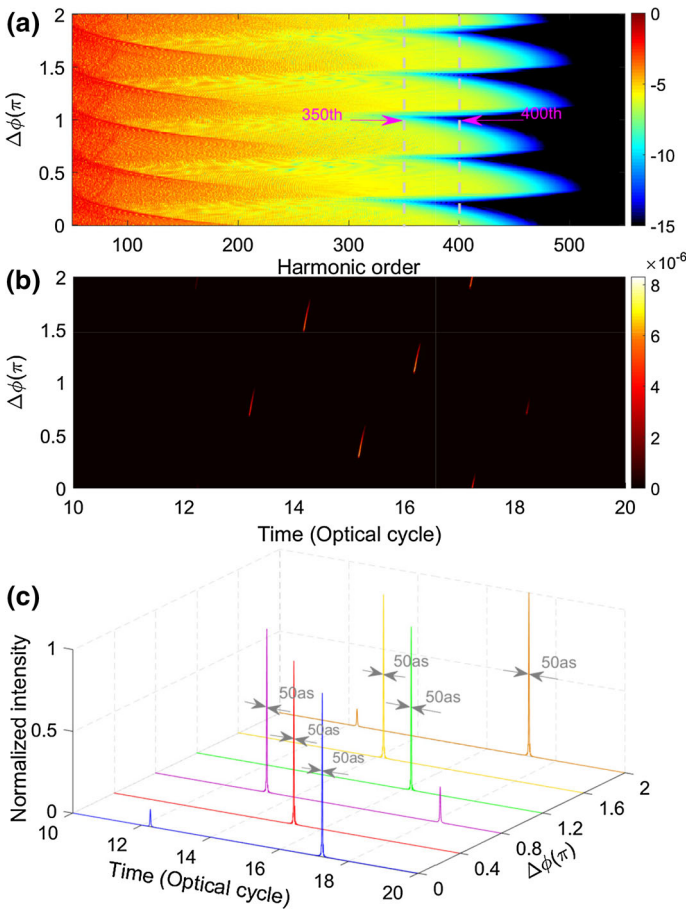


Fig. 5 (Color online) **a** The relative phase dependence of the generated harmonic spectrum in the multi-cycle two-color inhomogeneous field. The *color bar* shows the harmonic spectrum in a logarithmic scale. **b** The relative phase dependence of the IAP generated by synthesizing the harmonics from 543 eV (350th) to 620 eV (400th). **c** Temporal profiles of the IAPs with different relative phases (0π , 0.4π , 0.8π , 1.2π , 1.6π , 2.0π). In our simulations, except for $\Delta\phi$, other parameters are the same as that in Fig. 2

IAPs can be obtained for almost all the values of $\Delta\phi$ from 0 to 2π , except the range from 0.7π to 0.88π where the satellite attosecond pulses are generated around $18T_0$ to $18.5T_0$ with intensities less than 20% of that of the main attosecond pulses. Moreover, for $\Delta\phi$ around 0π (2π), the satellite attosecond pulses can be seen around $12T_0$. The intensities of the satellite attosecond pulses are about 10% of the main attosecond pulses around $17T_0$. They can be negligible when compared to the main ones (Takahashi et al. 2013). In Fig. 5c, we show the temporal profiles of the IAPs with $\Delta\phi = 0, 0.4\pi, 0.8\pi, 1.2\pi, 1.6\pi, 2.0\pi$. It is shown that the IAPs approaching to 50 as can be generated.

4 Conclusion

In conclusion, we propose a temporally and spatially shaped multi-cycle two-color field to produce IAPs in the water window region. The synthesized multi-cycle two-color field consists of a 30-fs, 800-nm (NIR) fundamental pulse and a 30-fs 2000-nm (MIR) control pulse. By using this two-color synthesis, the electron dynamics can be effectively controlled. Then a supercontinuum with the bandwidth of 233 eV (387–620 eV) is generated. Such a broadband supercontinuum can be successfully used to generate an isolated 40-as attosecond pulse. By enhancing the spatial inhomogeneity, the harmonic cutoff is extended to higher harmonics and the supercontinuum is broadened, which benefit the generation of the ultrashort IAPs. Moreover, the influence of the CEPs and the relative phase on the generation of IAPs has also been investigated. It shows that the broadband supercontinua with the bandwidths from 543 to 620 eV and IAPs with durations less than 80 as can be produced for almost all the values of CEPs and relative phases. Our two-color scheme is helpful to relax the requirement of CEP stabilization of the laser for the generation of IAP in the single-shot experiment. It must be emphasized that for HHG in inhomogeneous fields, the macroscopic propagation is insignificant due to the small propagation length in the nanostructure (Kim et al. 2008; Park et al. 2011; Sivis et al. 2013; Shaaran et al. 2013). The small volume of the nanostructure may limit the intensities of the emitted harmonics in our scheme.

Acknowledgements This work was supported by the National Natural Science Foundation of China under Grants Nos. 11404123 and 11422435. Numerical simulations presented in this paper were carried out using the High Performance Computing experimental testbed in SCTS/CGCL.

References

- Baltuška, A., Fuji, T., Kobayashi, T.: Controlling the carrier-envelope phase of ultrashort light pulses with optical parametric amplifiers. *Phys. Rev. Lett.* **88**(13), 133901 (2002)
- Cavaliere, A.L., Müller, N., Uphues, Th, Yakovlev, V.S., Baltuška, A., Horvath, B., Schmidt, B., Blümel, L., Holzwarth, R., Hendel, S., Drescher, M., Kleineberg, U., Echenique, P.M., Kienberger, R., Krausz, F., Heinzmann, U.: Attosecond spectroscopy in condensed matter. *Nature* **449**(7165), 1029–1032 (2007)
- Chang, Z., Rundquist, A., Wang, H., Murnane, M.M., Kapteyn, H.C.: Generation of coherent soft X-rays at 2.7 nm using high harmonics. *Phys. Rev. Lett.* **79**(16), 2967 (1997)
- Chang, Z.: Chirp of the single attosecond pulse generated by a polarization gating. *Phys. Rev. A* **71**(2), 023813 (2005)
- Ciappina, M.F., Aćimović, S.S., Shaaran, T., Biegert, J., Quidant, R., Lewenstein, M.: Enhancement of high harmonic generation by confining electron motion in plasmonic nanostructures. *Opt. Express* **20**(24), 26261–26274 (2012)
- Corkum, P.B.: Plasma perspective on strong field multiphoton ionization. *Phys. Rev. Lett.* **71**(13), 1994–1997 (1993)
- Corkum, P.B., Krausz, F.: Attosecond science. *Nat. Phys.* **3**(6), 381–387 (2007)
- Feit, M.D., Fleck, J.A., Steiger, A.: Solution of the Schrödinger equation by a spectral method. *J. Comput. Phys.* **47**(3), 412–433 (1982)
- Goulielmakis, E., Schultze, M., Hofstetter, M., Yakovlev, V.S., Gagnon, J., Uiberacker, M., Aquila, A.L., Gullikson, E.M., Attwood, D.T., Kienberger, R., Krausz, F., Kleineberg, U.: Single-cycle nonlinear optics. *Science* **320**(5883), 1614–1617 (2008)
- Goulielmakis, E., Loh, Z.H., Wirth, A., Santra, R., Rohringer, N., Yakovlev, V.S., Zherebtsov, S., Pfeifer, T., Azzeer, A.M., Kling, M.F., Leone, S.R., Krausz, F.: Real-time observation of valence electron motion. *Nature* **466**(7307), 739–743 (2010)
- Haessler, S., Balčiūnas, T., Fan, G., Andriukaitis, G., Pugžlys, A., Baltuška, A., Witting, T., Squibb, R., Zaïr, A., Tisch, J.W.G., Marangos, J.P.: Optimization of quantum trajectories driven by strong-field waveforms. *Phys. Rev. X* **4**(2), 021028 (2014)

- Haessler, S., Balčiūnas, T., Fan, G., Chipperfield, L.E., Baltuška, A.: Enhanced multi-colour gating for the generation of high-power isolated attosecond pulses. *Sci. Rep.* **5**, 10084 (2015)
- He, L., Wang, Z., Li, Y., Zhang, Q., Lan, P., Lu, P.: Wavelength dependence of high-order-harmonic yield in inhomogeneous fields. *Phys. Rev. A* **88**(5), 053404 (2013)
- He, M., Li, Y., Zhou, Y., Li, M., Lu, P.: Temporal and spatial manipulation of the recolliding wave packet in strong-field photoelectron holography. *Phys. Rev. A* **93**(3), 033406 (2016)
- Hentschel, M., Kienberger, R., Spielmann, Ch., Reider, G.A., Milosevic, N., Brabec, T., Corkum, P., Heinzmann, U., Drescher, M., Krausz, F.: Attosecond metrology. *Nature* **414**(6863), 509–513 (2001)
- Itatani, J., Levesque, J., Zeidler, D., Niikura, H., Pépin, H., Kieffer, J.C., Corkum, P.B., Villeneuve, D.M.: Tomographic imaging of molecular orbitals. *Nature* **432**(7019), 867–871 (2004)
- Ke, S., Wang, B., Long, H., Wang, K., Lu, P.: Topological edge modes in non-Hermitian plasmonic waveguide arrays. *Opt. Express* **25**(10), 11132–11143 (2017)
- Kienberger, R., Goulielmakis, E., Uiberacker, M., Baltuska, A., Yakovlev, V., Bammer, F., Scrinzi, A., Westerwalbesloh, Th, Kleineberg, U., Heinzmann, U., Drescher, M., Krausz, F.: Atomic transient recorder. *Nature* **427**(6977), 817–821 (2004)
- Kim, S., Jin, J., Kim, Y.J., Park, I.Y., Kim, Y., Kim, S.W.: High-harmonic generation by resonant plasmon field enhancement. *Nature* **453**(7196), 757–760 (2008)
- Kim, S., Jin, J., Kim, Y.J., Park, I.Y., Kim, Y., Kim, S.W.: Kim et al. reply. *Nature* **485**(7397), E1–E3 (2012)
- Krausz, F., Ivanov, M.: Attosecond physics. *Rev. Mod. Phys.* **81**(1), 163–234 (2009)
- Lan, P., Lu, P., Cao, W., Li, Y., Wang, X.: Isolated sub-100-as pulse generation via controlling electron dynamics. *Phys. Rev. A* **76**(1), 011402 (2007)
- Lan, P., Lu, P., Li, Q., Li, F., Hong, W., Zhang, Q.: Macroscopic effects for quantum control of broadband isolated attosecond pulse generation with a two-color field. *Phys. Rev. A* **79**(4), 043413 (2009)
- Lan, P., Takahashi, E.J., Midorikawa, K.: Optimization of infrared two-color multicycle field synthesis for intense-isolated-attosecond-pulse generation. *Phys. Rev. A* **82**(5), 053413 (2010)
- Li, L., Wang, Z., Li, F., Long, H.: Efficient generation of highly elliptically polarized attosecond pulses. *Opt. Quantum Electron.* **49**(2), 73 (2017a)
- Li, Y., Li, M., Zhou, Y., Ma, X., Xie, H., Lan, P., Lu, P.: Carrier-envelope phase dependent photoelectron energy spectra in low intensity regime. *Opt. Express* **25**(10), 11233–11243 (2017b)
- Li, L., Zhu, X., Lan, P., Li, X., Lu, P.: Photon channel perspective on high harmonic generation. [arXiv:1702.04084](https://arxiv.org/abs/1702.04084) [physics.atom-ph] (2017c)
- Liu, X., Li, P., Zhu, X., Lan, P., Zhang, Q., Lu, P.: Probing the $\pi-\pi^*$ transitions in conjugated compounds with an infrared femtosecond laser. *Phys. Rev. A* **95**(3), 033421 (2017a)
- Liu, Q., Wang, B., Ke, S., Long, H., Wang, K., Lu, P.: Exceptional points in Fano-resonant graphene metamaterials. *Opt. Express* **25**(7), 7203–7212 (2017b)
- Luo, J., Li, Y., Wang, Z., Zhang, Q., Lu, P.: Ultra-short isolated attosecond emission in mid-infrared inhomogeneous fields without CEP stabilization. *J. Phys. B* **46**(14), 145602 (2013)
- Ma, X., Li, M., Zhou, Y., Lu, P.: Nonsequential double ionization of Xe by mid-infrared laser pulses. *Opt. Quantum Electron.* **49**(4), 170 (2017)
- Park, I.Y., Kim, S., Choi, J., Lee, D.H., Kim, Y.J., Kling, M.E., Stockman, M.I., Kim, S.M.: Plasmonic generation of ultrashort extreme-ultraviolet light pulses. *Nat. Photon* **5**(11), 677–681 (2011)
- Paul, P.M., Toma, E.S., Breger, P., Mullot, G., Augé, F., Balcou, Ph, Muller, H.G., Agostini, P.: Observation of a train of attosecond pulses from high harmonic generation. *Science* **292**(5522), 1689–1692 (2001)
- Pérez-Hernández, J.A., Ciappina, M.F., Lewenstein, M., Roso, L., Zair, A.: Beyond carbon k-edge harmonic emission using a spatial and temporal synthesized laser field. *Phys. Rev. Lett.* **110**(5), 053001 (2013)
- Pfeifer, T., Gallmann, L., Abel, M.J., Nagel, P.M., Neumark, D.M., Leone, S.R.: Heterodyne mixing of laser fields for temporal gating of high-order harmonic generation. *Phys. Rev. Lett.* **97**(16), 163901 (2006)
- Popmintchev, T., Chen, M.C., Popmintchev, D., Arpin, P., Brown, S., Ališauskas, S., Andriukaitis, G., Balčiūnas, T., Mücke, O.D., Pugzlys, A., Baltuška, A., Shim, B., Schrauth, S.E., Gaeta, A., Hernández-García, C., Plaja, L., Becker, A., Jaron-Becker, A., Murnane, M.M., Kapteyn, H.C.: Bright coherent ultrahigh harmonics in the keV X-ray regime from mid-infrared femtosecond lasers. *Science* **336**(6086), 1287–1291 (2012)
- Qin, M., Zhu, X.: Molecular orbital imaging for partially aligned molecules. *Opt. Laser Technol.* **87**, 79–86 (2017)
- Sansone, G., Benedetti, E., Calegari, F., Vozzi, C., Avaldi, L., Flammini, R., Poletto, L., Villoresi, P., Altucci, C., Velotta, R., Stagira, S., De Silvestri, S., Nisoli, M.: Isolated single-cycle attosecond pulses. *Science* **314**(5798), 443–446 (2006)
- Sharan, T., Ciappina, M.F., Guichard, R., Pérez-Hernández, J.A., Roso, L., Arnold, M., Siegel, T., Zair, A., Lewenstein, M.: High-order-harmonic generation by enhanced plasmonic near-fields in metal nanoparticles. *Phys. Rev. A* **87**(4), 041402 (2013)

- Sivis, M., Duwe, M., Abel, B., Ropers, C.: Nanostructure-enhanced atomic line emission. *Nature* **485**(7397), E1–E3 (2012)
- Sivis, M., Duwe, M., Abel, B., Ropers, C.: Extreme-ultraviolet light generation in plasmonic nanostructures. *Nat. Phys.* **9**(5), 304–309 (2013)
- Takahashi, E.J., Kanai, T., Ishikawa, K.L., Nabekawa, Y., Midorikawa, K.: Coherent water window X-ray by phase-matched high-order harmonic generation in neutral media. *Phys. Rev. Lett.* **101**(25), 253901 (2008)
- Takahashi, E.J., Lan, P., Mütcke, O.D., Nabekawa, Y., Midorikawa, K.: Infrared two-color multicycle laser field synthesis for generating an intense attosecond pulse. *Phys. Rev. Lett.* **104**(23), 233901 (2010)
- Takahashi, E.J., Lan, P., Mücke, O.D., Nabekawa, Y., Midorikawa, K.: Attosecond nonlinear optics using gigawatt-scale isolated attosecond pulses. *Nat. Commun.* **4**, 2691 (2013)
- Teichmann, S.M., Silva, F., Cousin, S.L., Hemmer, M., Biegert, J.: 0.5-keV soft X-ray attosecond continua. *Nat. Commun.* **7**, 11493 (2016)
- Yavuz, I., Bleda, E.A., Altun, Z., Topcu, T.: Generation of a broadband xuv continuum in high-order-harmonic generation by spatially inhomogeneous fields. *Phys. Rev. A* **85**(1), 013416 (2012)
- Zhai, C., He, L., Lan, P., Zhu, X., Li, Y., Wang, F., Shi, W., Zhang, Q., Lu, P.: Coulomb-corrected molecular orbital tomography of nitrogen. *Sci. Rep.* **6**, 23236 (2016)
- Zhai, C., Zhu, X., Lan, P., Wang, F., He, L., Shi, W., Li, Y., Li, M., Zhang, Q., Lu, P.: Diffractive molecular-orbital tomography. *Phys. Rev. A* **95**(3), 033420 (2017)
- Zhao, D., Wang, Z., Long, H., Wang, K., Wang, B., Lu, P.: Optical bistability in defective photonic multilayers doped by graphene. *Opt. Quantum Electron.* **49**(4), (2017)
- Zhang, X., Zhu, X., Liu, X., Wang, D., Zhang, Q., Lan, P., Lu, P.: Ellipticity-tunable attosecond XUV pulse generation with a rotating bichromatic circularly polarized laser field. *Opt. Lett.* **42**(6), 1027–1030 (2017)
- Zhou, Y., Li, M., Li, Y., Tong, A., Li, Q., Lu, P.: Dissection of electron correlation in strong-field sequential double ionization using a classical model. *Opt. Express* **25**(7), 8450–8458 (2017)
- Zhu, X., Lan, P., Liu, K., Li, Y., Liu, X., Zhang, Q., Barth, I., Lu, P.: Helicity sensitive enhancement of strong-field ionization in circularly polarized laser fields. *Opt. Express* **24**(4), 4196–4209 (2016)